Theoretical Studies
on Quantum Walks with a Time-varying Coin

Haruna Katayama   Noriyuki Hatakenaka   Toshiyuki Fujii

Graduate School of Integrated Arts and Sciences   Department of Physics
Hiroshima University   Asahikawa Medical University
Hiroshima, Japan   Hokkaido, Japan

`halna496@gmail.com`   `noriyuki@hiroshima-u.ac.jp`   `tfujii@asahikawa-med.ac.jp`

Quantum walks can reconstruct quantum algorithms for quantum computation, where the precise controls of quantum state transfers between arbitrary distant sites are required. Here, we investigate quantum walks using a periodically time-varying coin both numerically and analytically, in order to explore the controllability of quantum walks while preserving its random nature.

1 Introduction

The quantum computer promises drastically fast processing using quantum algorithms based on unique features of quantum mechanics. Just as classical random walks have been used to design computational algorithms in computer science, quantum walks[1] also have been used to reconstruct algorithms suitable for quantum mechanics and play an incredibly important role in quantum information processing and computation protocols[6, 11].

A state transfer is required in such quantum algorithms. It is, however, difficult to control the state transfer because the quantum walk is inherently random[5, 9, 16, 17]. One of the propositions to solve this problem is a coin that has a part in determining the movement of the quantum walk. Wojcik et al. extended the coins that previously, were spatially constant to space-dependent coins[14]. Bañuls et al. diversified their work further into the time domain, led to a more generalized quantum walk[3]. They found that a time-varying coin[2, 3, 4, 7, 12, 13, 15] can modify trajectories of the quantum walks. This implies that quantum walks are controllable.

In this paper, we present that the time-varying coins can control the trajectories on demand while preserving random processes. First, we numerically show that the trajectories can be surely modified by using the simplest time-varying coin, i.e., linear time dependent coin. Then, we discuss on the walking mechanism using the analytic solution derived by means of the long-wavelength approximation method by Knight, Roldán, and Sipe[10]. Moreover, we investigate quantum walks with another important coin which is more general time-dependent in both numerical and analytical perspective, leading to the controllability of the quantum walks by the time-varying coins. Controlling the quantum walks can improve the quantum algorithm to be more efficient.

2 Quantum walk with a time-varying coin

Let us consider a quantum walk with *a time-varying coin* on a line. In random walks, the walker moves one step to right or left depending on the outcome of the coin toss. A quantum walk is a quantum-mechanical counterpart of the classical random walk. Then, a quantum walk lives in a bipartite system comprising positions and coin degrees of freedom represented as an entire Hilbert space $\mathscr{H} = \mathscr{H}_p \otimes \mathscr{H}_c$,

where $\mathscr{H}_p$ and $\mathscr{H}_c$ are the Hilbert spaces of the walker's position and the coin spanned by $\{|m\rangle, m \in \mathbb{Z}\}$ and $\{|R\rangle, |L\rangle\}$, respectively. The walker's behaviour is characterized by both the coin and the shift operators. The time-varying coin *unitary* operator employed in this paper is defined as

$$\hat{C} = \begin{pmatrix} \cos(\theta(t)) & \sin(\theta(t)) \\ \sin(\theta(t)) & -\cos(\theta(t)) \end{pmatrix}, \tag{1}$$

which transforms the internal state of a coin through a time-varying phase $\theta(t)$. On the other hand, the shift operator given by

$$\hat{S}|m,R\rangle = |m+1,R\rangle, \tag{2}$$

$$\hat{S}|m,L\rangle = |m-1,L\rangle, \tag{3}$$

shifts the walker's position.

The state after n steps $|\psi\rangle_n$ is described by

$$|\psi\rangle_n = (\hat{S}\hat{C})^n |\psi\rangle_0, \tag{4}$$

where $|\psi\rangle_0$ represents the walker's initial state. This is also re-expressed by

$$|\psi\rangle_n = \sum_{m=-n}^{n} [R_{m,n}|m,R\rangle + L_{m,n}|m,L\rangle], \tag{5}$$

if we introduce $|R(L)_{m,n}|^2$ representing the probability of being in the internal state $R(L)$ at position m after n steps. Here, the probability amplitudes $R_{m,n}$ and $L_{m,n}$ at position m after n steps are determined by

$$R_{m,n+1} = \cos\theta_n R_{m-1,n} + \sin\theta_n L_{m-1,n}, \tag{6}$$

$$L_{m,n+1} = \sin\theta_n R_{m+1,n} - \cos\theta_n L_{m+1,n}, \tag{7}$$

where $\theta_n = \theta(nT)$ with T being the time interval between steps. Therefore, the probability of finding the walker at position m after n steps $P_m(n)$ is described by

$$P_m(n) = P_m^R(n) + P_m^L(n), \tag{8}$$

$$P_m^R(n) = |R_{m,n}|^2, \quad P_m^L(n) = |L_{m,n}|^2. \tag{9}$$

3 Linear time evolution of the phase in the coin operator

Here, let us discuss the linear time evolution of the phase, i e., $\theta(t) = \theta_0 + \omega t$ in the coin operator as the simplest example of time-varying coins. Through this example, we will extract the essential properties of a quantum walk with a time-varying coin and elucidate the walking mechanism.

3.1 Numerical approaches

Numerical simulations are carried out by using $\theta(t) = \theta_0 + \omega t$ as a specific time-dependent expression of the coin operator in Eq. (1) with various values for the initial phase θ_0 and the frequency ω. Figure 1 (A), (B) and (C) show the probability distributions of finding a walker on a line as a function of time under the identical frequency $\omega = \pi/60$ (upper panels) and their *walker's trajectories* representing the place

where the existence probability is high (lower panels). It is found that the time-varying coin leads to periodic walker's trajectories classified into three types depending on the initial phase of the coin θ_0: (1) **Loop-line chain** which is composed of loops and lines appearing alternately as shown in Fig. 1(A), (2) **Crossing loop-loop chain** where two major trajectories intersect as shown Fig. 1 (B), and (3) **Touching loop-loop chain** where two major trajectories come into contact as shown in Fig. 1 (C). In addition, walker's trajectories are also modified by the frequency ω. As the frequency ω increases, the size of the loops tends to become smaller in time and narrower in space (not displayed in Fig. 1).
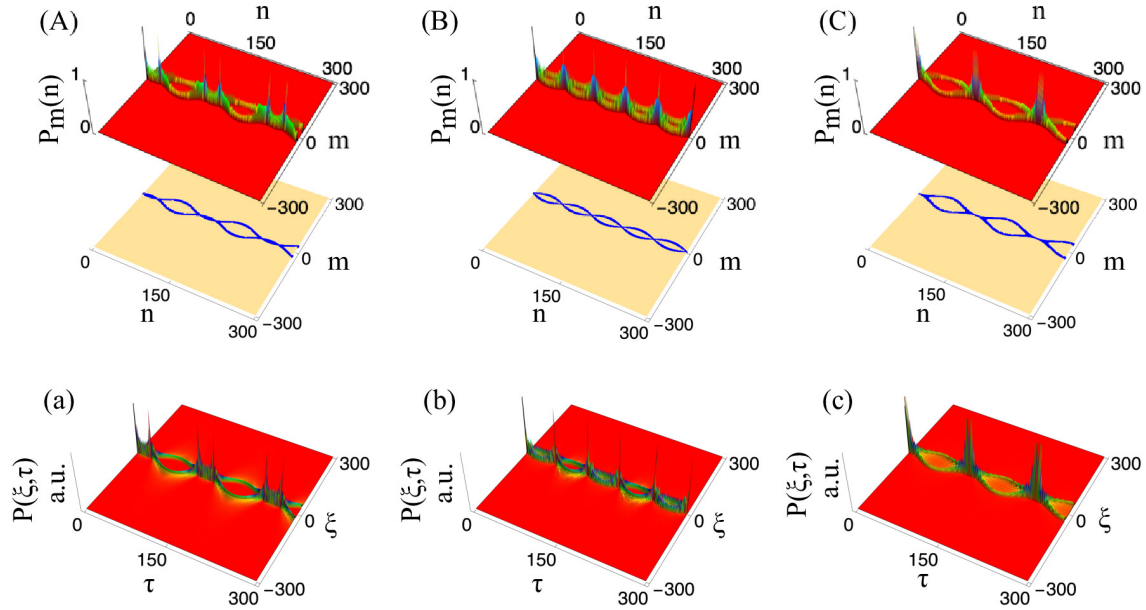

Figure 1: Probability distributions obtained by numerical simulations (upper panels) and their walker's trajectories (lower panels) for quantum walks over 300 steps with the time interval between steps $T = 1$ and initial state $|\psi\rangle_0 = |0,R\rangle / \sqrt{2} + i|0,L\rangle / \sqrt{2}$, for various initial phases (A)$\theta_0 = \pi/4$, (B)$\theta_0 = 0$, and (C)$\theta_0 = 3\pi/2$ under the fixed coin's frequency $\omega = \pi/60$. The corresponding analytical solutions are given in (a), (b) and (c) of the bottom panels.

3.2 Analytical approach

In order to explore the physical origin of walker's trajectories obtained by numerical simulations in the previous section, analytical probability distributions are obtained according to the method proposed by Knight, Roldán and Sipe[10]. Equations (6) and (7) are reduced to the following recurrence formula,

$$A_{m,n+1} - A_{m,n-1} = -\cos\theta_n(A_{m+1,n} - A_{m-1,n}), \tag{10}$$

where $\theta_n = \theta_0 + n\omega T$ and $A = R, L$. In the long-wavelength approximation, we obtain the wave equation for the continuous function $A(x,t)$

$$T\frac{\partial}{\partial t}A(x,t) = -\cos\theta(t)\left(X\frac{\partial}{\partial x} + \frac{X^3}{3!}\frac{\partial^3}{\partial x^3}\right)A(x,t). \tag{11}$$

where X stands for the distance between steps. We further introduce other two fields $A^+(\xi,\tau)$ and $A^-(\xi,\tau)$ to express the waves spreading in both sides on a line, resulting in the wave equation

$$\frac{\partial}{\partial\tau}A^\pm(\xi,\tau) = \mp\cos\theta(\tau)\left(\frac{\partial}{\partial\xi} + \frac{1}{3!}\frac{\partial^3}{\partial\xi^3}\right)A^\pm(\xi,\tau), \tag{12}$$

where $\xi = x/X$ and $\tau = t/T$. This differential equation can be solved using Fourier techniques after separation of variables in a usual manner. The solution for Eq. (12) are given as follows

$$A^\pm(\xi,\tau) = \frac{1}{2}\sum_m(A_{m,0}\pm A_{m,1})Z^\pm(\xi - m,\tau), \tag{13}$$

with

$$Z^\pm(\xi,\tau) = \left|\frac{2}{s(\tau)}\right|^{\frac{1}{3}}e^\chi\,\mathrm{Ai}(\zeta), \tag{14}$$

$$\zeta = \left|\frac{2}{s(\tau)}\right|^{\frac{1}{3}}\left(\pm\xi - s(\tau) + \frac{2w^4}{s(\tau)}\right), \tag{15}$$

$$\chi = \frac{2w^2}{s(\tau)}\left(\pm\xi - s(\tau) + \frac{4w^4}{3s(\tau)}\right), \tag{16}$$

$$s(\tau) = \mp\int_0^\tau\cos\theta(\tau')d\tau', \tag{17}$$

where Ai represents the Airy function. The probability distribution of finding a walker is then given by

$$P(\xi,\tau) = P^R(\xi,\tau) + P^L(\xi,\tau), \tag{18}$$

$$P^A(\xi,\tau) = |A^+(\xi,\tau) + (-1)^nA^-(\xi,\tau)|^2. \tag{19}$$

Figure 1 (a), (b) and (c) show probability distributions depicted by the analytic solution for the same value as coin parameters used in numerical simulations to (A), (B) and (C), respectively. Our analytical solution reproduces the numerical simulation well.

One definite example is as follows. Figure 2 shows the top view of the probability distributions obtained by the analytical solution (left) and the numerical simulation (right) at $\theta_0 = 0$ and $\omega = \pi/60$. According to the probability distribution given analytically in Eq.(18), the probability $P(\xi,\tau)$ is composed of $P^R(\xi,\tau)$ and $P^L(\xi,\tau)$. The highest probabilities in the analytical probability distribution are highlighted in blue ($P^R(\xi,\tau)$) and red ($P^L(\xi,\tau)$). The blue line and red line are exactly intersecting at $\tau = 60$ with the same amplitude, resulting in a crossing loop-loop chain as seen in the numerical simulation. Actually, there exists a slight difference between analytical solutions and numerical simulations. Specifically, the amplitudes of the first and second loops differ only slightly in the graph on the left of Fig. 2. This is due to the approximation limit based on the wave nature of the quantum walk, i e., the nature of the Airy function. The maximum peak of the Airy function $\mathrm{Ai}(x)$ is not located at $x = 0$, but at slightly negative position. As a result, the blue peak shifts more negatively than the dotted green line, and the red peak does the opposite. In other words, the maximum peak exists at the inside of the numerical loop at $\tau = 30$, and outside at $\tau = 90$ because the direction of the Airy function is reversed. This tiny difference causes only a few deviations. Thus, the analytical solution approximates the numerical simulation well. However, the linear spreading inherent in the quantum walk is not reproduced in the analytical solution and remains unsolved.

Despite the above better agreement, the probability distribution shown in Fig. 1 (b) may look different from that of numerical simulation shown in Fig. 1 (B). This difference is due to the Poggendorff illusion[8], which is a geometrical-optical illusion that involves the brain's perception of the interaction between diagonal lines and horizontal and vertical edges. In fact, the probability of being inward in the first (left) loop and outward in the second (right) loop causes the Poggendorff illusion. In contrast, the numerical simulation does not show such a difference, resulting in no Poggendorff illusion. From the above, the analytic solution seemed to be different from the probability distribution of the numerical simulation, but in fact the analytic solution could approximate the numerical simulation correctly.
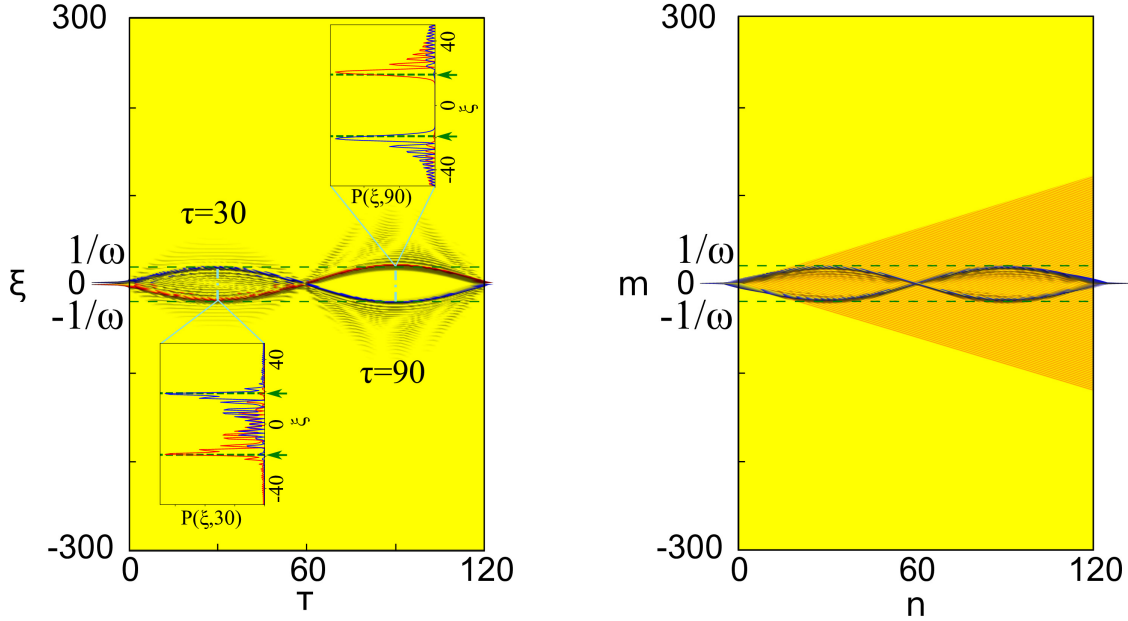

Figure 2: Top views of the probability distributions depicted in Fig.1 (B) and (b) over 120 steps. The analytical probability distributions are shown on the left, where the high probabilities formed by $P^R(\xi,\tau)$ and $P^L(\xi,\tau)$ are highlighted in blue and red with shaded lower existence probability. Two embedded figures represent the sectional view of the probability distribution at $\tau = 30$ and $\tau = 90$, respectively. The numerical probability distribution displayed on the right is formed by a trail with high probabilities highlighted in blue and a triangular area with low probabilities highlighted in orange, which are not drawn in Fig. 1(B) due to the accuracy of the color gradation. The values of the probability distributions are equal to zero in yellow area of both diagrams. The doted lines in both diagrams represent the amplitude of the walker's trajectory given analytically in Eq. (22)

3.3   Waking mechanism

Now, let us discuss the walking mechanism based on the analytical solutions supported by numerical simulations obtained above. To find the walker's trajectories which are a key clue for elucidating the walking mechanism, we examine the behavior of the probability amplitude $A^{\pm}(\xi,\tau)$, which is the main element that determines the probability distribution. The amplitude $A^{\pm}(\xi,\tau)$ is expressed as follows:

$$A^{\pm}(\xi, \tau) = \int_{-\infty}^{\infty} e^{ik\xi} A^{\pm}(k, \tau) dk$$

$$= B^{\pm} \left(\xi \mp \int_{0}^{\tau} \cos\theta(\tau')d\tau', \tau \right), \tag{20}$$

where $B^{\pm}(\xi, \tau)$ represents a shifted probability amplitude described by

$$B^{\pm}(\xi, \tau) = \int_{-\infty}^{\infty} e^{ik\xi} \left(e^{\pm\frac{1}{6}ik^3 \int_0^\tau \cos\theta(\tau')d\tau'} A^{\pm}(k, 0) \right) dk. \tag{21}$$

Therefore, the walker's trajectories is analytically obtained by the shift in Eq. (20) as follows:

$$x_c = \mp \int_{0}^{\tau} \cos\theta(\tau')d\tau'$$

$$= \mp \left(\frac{1}{\omega} \sin(\theta_0 + \omega\tau) - \frac{1}{\omega} \sin\theta_0 \right). \tag{22}$$

Equation (22) means that walker's trajectories are composed of two antisymmetric sinusoidal functions with same parameters such as amplitude $1/\omega$, initial phase θ_0, frequency ω, and bias $-\sin\theta_0/\omega$. The walker's trajectories are formed by overlap of two sinusoidal waves, and are classified into three categories like loop-line chains, crossing loop-loop chains, and touching loop-loop chains as seen in numerical simulations. According to our simple overlap model, these three types of chains are interpreted as follows. Figure 3 (a) shows the first type of walker's trajectories named "loop-line chain". In fact, two different size loops appear alternately though loop and line seemed to appear alternately. This type of chains is generated when the bias is finite except for $\theta_0 = n\pi/2, (n =$integer). Figure 3 (b) shows the second type of walker's trajectories, named "crossing loop-loop chain". This type of chains occurs when the bias is equal to 0, equivalently $\theta_0 = n\pi$. Figure 3 (c) shows the third type of walker's trajectories "touching loop-loop chain", which appears when the sinusoidal-wave amplitude equals its bias $(\theta_0 = (2n+1)\pi/2)$. In this way, based on our analytical solution, it is found that walker's trajectories are classified into three depending on the θ_0 as obtained by numerical simulation.

The walker's trajectories reflecting the walking mechanism reveal its physical origin. A trajectory is, in general, simply described by $\int v(t)dt$ wiht $v(t)$ being time-dependent velocity. According to wave theory, the velocity $v(t)$ works to connect the wave number k (space) and frequency ω (time) through the well-known dispersion relation $\omega = vk$ in the linear wave. From our wave equation, Eq.(12), the term $\mp \cos\theta(\tau)$ corresponds to the wave velocity. In other words, the velocity that determines the trajectory is nothing but the transition amplitude of the coin itself. This shows that the time-varying coin parameter, i.e., the wave velocity, controls the walker's trajectories. This is our central result of this paper.

4 Sinusoidal time evolution of the phase in the coin operator

In the previous section, we have revealed the walking mechanism of the quantum walk with a time-varying coin for the simplest example. Here let us apply this mechanism to other time-varying coin such as $\theta(t) = \theta_0 \sin(\omega t)$. This is considered to be a great clue for extending to coins with general time dependence because $\theta_0 \sin(\omega t)$ is a component of the Fourier series expansion which describes general time dependences.
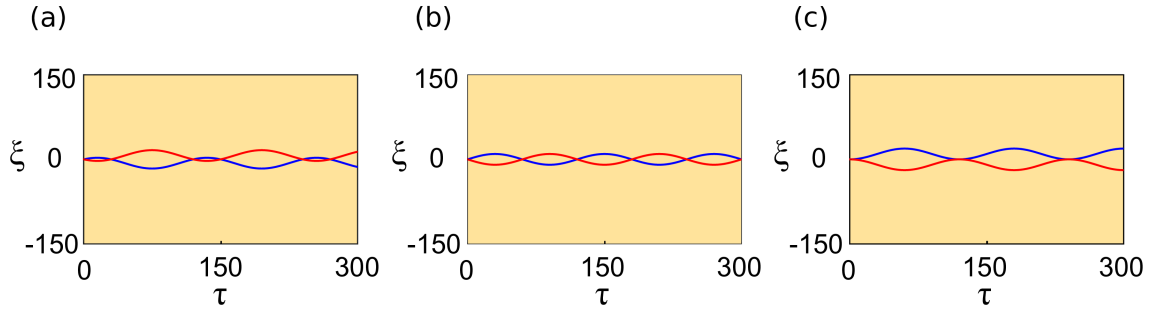
Figure 3: Three types of walker's trajectories depicted by the analytic solution for the quantum walk over 300 steps with a time-varying coins for identical coin frequency $\omega = \pi/60$ (a) a loop-line chain emerging with $\theta_0 = \pi/4$ (b) a crossing loop-loop chain emerging with $\theta_0 = n\pi$ (c) a touching loop-loop chain emerging with $\theta_0 = (2n+1)\pi/2$

The analytic solutions Eqs. (13)-(17) are derived parallel to the previous section. Figure 4 shows the probability distribution obtained both numerically and analytically. The analytical solutions agree well with the numerical simulations. The walker's trajectory is similarly obtained by

$$x_c = \mp \int_0^\tau \cos\left(\theta_0 \sin(\omega\tau')\right) d\tau'$$
$$= \mp \left\{ J_0(\theta_0)\tau + \sum_{k=1}^\infty J_{2k}(\theta_0) \sin(2k\omega\tau)) \right\} \tag{23}$$

where $J_k(\theta_0)$ is the Bessel function of the first kind of order k of θ_0. The walker's trajectory spreads linearly owing to the first term $J_0(\theta_0)\tau$ in Eq. (23), and fluctuates periodically around the linear term due to the rest of the other terms. In practice, the trajectory can be described accurately with only a few terms in the summation due to the Bessel functions. As a result, it is found that our walking mechanism can be applicable to the walker's trajectories on the quantum walk with more general time-varying coin. More general extensions will appear elsewhere.

5   Conclusion

We have investigated quantum walks with a time-varying coin, in order to explore the controllability of quantum walks for efficient implementations of quantum state transfers in quantum walk-based quantum computers. Our numerical simulations have revealed the key fundamental behaviour behind the time-varying coined quantum walk through the walker's trajectory analysis at the simplest linear time-varying coin. Then, an analytical solution based on the wave nature of the quantum walk has unraveled the walking mechanism that the wave velocity of the quantum walk is governed by the time-varying coin parameter. This mechanism has been shown to be applicable to more important time-varying coins such as sinusoidal functions. Therefore, the walking mechanism enables us to control quantum walks by manipulating coin parameters. The designed time-varying coined quantum walk opens a new pathway for manipulating quantum state transfers in quantum information technology.
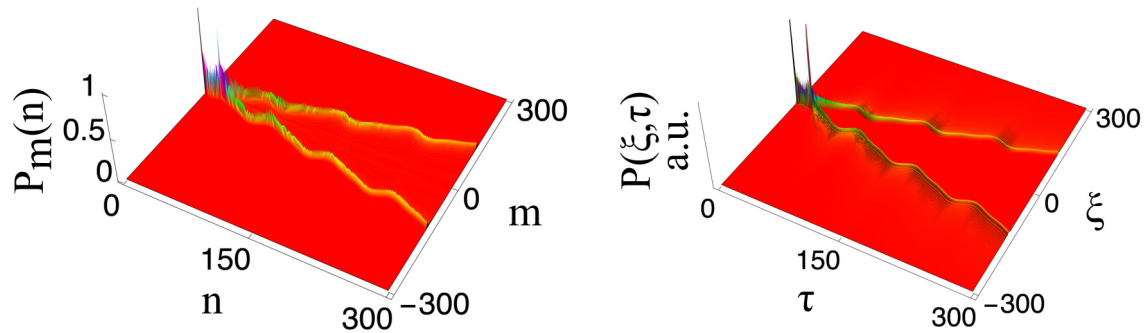
Figure 4: Probability distributions obtained numerically (left) and analytically (right) for quantum walks over 300 steps with the time-varying coin $\theta(t) = (5\pi/4)\sin(\pi t/80)$ and initial state $|\psi\rangle_0 = |0, R\rangle/\sqrt{2} + i|0, L\rangle/\sqrt{2}$. The other parameters are the same as in Fig. 1.

References

[1] Y. Aharonov, L. Davidovich & N. Zagury (1993): *Quantum random walks*. *Phys. Rev. A* 48, pp. 1687–1690, doi:10.1103/PhysRevA.48.1687.

[2] Francesca Albertini & Domenico DAlessandro (2009): *Analysis of quantum walks with time-varying coin on d-dimensional lattices*. *Journal of Mathematical Physics* 50(12), p. 122106, doi:10.1063/1.3271109.

[3] Mari-Carmen Bañuls, C. Navarrete, A. Pérez, Eugenio Roldán & J. Soriano (2006): *Quantum Walk with a time-dependent coin*. *Physical Review A* 73(6), doi:10.1103/PhysRevA.73.062304.

[4] C. Cedzich & R. F. Werner (2016): *Revivals in quantum walks with a quasiperiodically-time-dependent coin*. *Physical Review A* 93(3), doi:10.1103/physreva.93.032329.

[5] Tian Chen, Bo Wang & Xiangdong Zhang (2017): *Controlling probability transfer in the discrete-time quantum walk by modulating the symmetries*. *New Journal of Physics* 19(11), p. 113049, doi:10.1088/1367-2630/aa8fe4.

[6] Andrew M. Childs (2009): *Universal Computation by Quantum Walk*. *Phys. Rev. Lett.* 102, p. 180501, doi:10.1103/PhysRevLett.102.180501.

[7] Giuseppe Di Molfetta, Lauchlan Honter, Ben B. Luo, Tatsuaki Wada & Yutaka Shikano (2015): *Massless Dirac equation from Fibonacci discrete-time quantum walk*. *Quantum Studies: Mathematics and Foundations* 2(3), p. 243, doi:10.1007/s40509-015-0038-6.

[8] Suzanne Greist-Bousquet & Harvey R Schiffman (1981): *The Poggendorff Illusion: An Illusion of Linear Extent?* *Perception* 10(2), pp. 155–164, doi:10.1068/p100155. PMID: 7279544.

[9] Michal Karski, Leonid Förster, Jai-Min Choi, Andreas Steffen, Wolfgang Alt, Dieter Meschede & Artur Widera (2009): *Quantum Walk in Position Space with Single Optically Trapped Atoms*. *Science* 325(5937), pp. 174–177, doi:10.1126/science.1174436.

[10] Peter L. Knight, Eugenio Roldán & J. E. Sipe (2004): *Propagating quantum walks: The origin of interference structures*. *Journal of Modern Optics* 51(12), p. 1761, doi:10.1080/09500340408232489.

[11] Neil B. Lovett, Sally Cooper, Matthew Everitt, Matthew Trevers & Viv Kendon (2010): *Universal quantum computation using the discrete-time quantum walk*. *Physical Review A* 81(4), doi:10.1103/physreva.81.042330.

[12] S Panahiyan & S Fritzsche (2018): *Controlling quantum random walk with a step-dependent coin*. *New Journal of Physics* 20(8), p. 083028, doi:10.1088/1367-2630/aad899.

[13] Y. Shikano, T. Wada & J. Horikawa (2014): *Discrete-time quantum walk with feed-forward quantum coin*. *Scientific Reports* 4, doi:10.1038/srep04427.

[14] Antoni Wójcik, Tomasz Łuczak, Paweł Kurzyński, Andrzej Grudka & Małgorzata Bednarska (2004): *Quasiperiodic dynamics of a quantum walk on the line*. *Physical review letters* 93(18), p. 180601, doi:10.1038/nature02008.

[15] P. Xue, R. Zhang, H. Qin, X. Zhan, Z. H. Bian, J. Li & Barry C. Sanders (2015): *Experimental Quantum-Walk Revival with a Time-Dependent Coin*. *Phys. Rev. Lett.* 114, p. 140502, doi:10.1103/PhysRevLett.114.140502.

[16] İskender Yalçınkaya & Zafer Gedik (2015): *Qubit state transfer via discrete-time quantum walks*. *Journal of Physics A: Mathematical and Theoretical* 48(22), p. 225302, doi:10.1088/1751-8113/48/22/225302.

[17] Xiang Zhan, Hao Qin, Zhi-hao Bian, Jian Li & Peng Xue (2014): *Perfect state transfer and efficient quantum routing: A discrete-time quantum-walk approach*. *Phys. Rev. A* 90, p. 012331, doi:10.1103/PhysRevA.90.012331.